Synergistic amalgamation of ZIF-8 into ZIF-67 framework for enhanced supercapacitor application

Emeka Oparaku¹, Chidiebere O. Obasi¹, Ekene Uduike¹, Imosobomeh L. Ikhioya^{1,2}

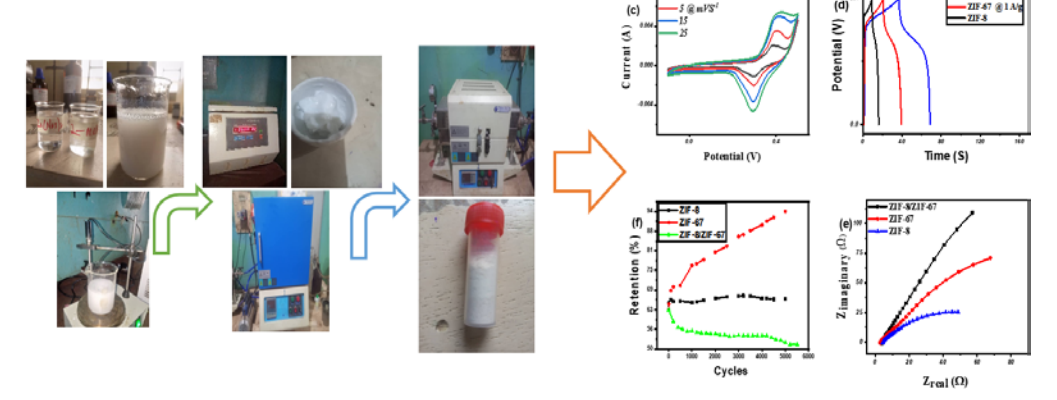
¹Department of Physics and Astronomy, University of Nigeria, Nsukka, 410001, Nigeria. ²Department of Physics, Federal University Lokoja, PMB 1154, Kogi State, Nigeria.

Submitted on: 06-May-2025, Revised: 30-Jun-2025, Accepted on: 01-Jul-2025, and Published on: 02-Jul-2025

Article

ABSTRACT

This study employed a direct combination method to synthesize ZIF-8, ZIF-67, and a ZIF-8/ZIF-67 composite. Using electrochemical impedance spectroscopy (EIS), galvanostatic charge-discharge (GCD), and cyclic voltammetry (CV), the



charge storage behavior of the prepared electrode was investigated through electrochemical analysis. ZIF-8, ZIF-67, and ZIF-8/ZIF-67 have specific capacitances of 223, 255, and 609 F/g, respectively. The ZIF-8, ZIF-67, and ZIF-8/ZIF-67 electrodes had energy densities of 15.8, 38.8, and 69 Wh/kg, respectively. The power density of ZIF-8, ZIF-67, and ZIF-8/ZIF-67 electrodes was determined to be (469.41, 745.64, and 779) W/kg at a current density of 1 A/g. The retention plot of ZIF-8, ZIF-67, ZIF-8/ZIF-67 electrodes show efficiency of 65%, 92% and 63%, respectively, indicating their suitability for supercapacitor applications. The bandgap energies of ZIF-8 (2.50 eV) and ZIF-67 (2.77 eV) indicate their potential as semiconductors in electronic applications, with ZIF-67 having a higher energy and thus greater electronic characteristics. The composite ZIF-8/ZIF-67 has a reduced bandgap (2.35 eV), indicating increased charge carrier mobility due to the mixing of frameworks. The XRD diffraction peaks at 22.09° (110), 26.62° (200), 38.49° (211), and 47.27° (220) correspond to unique crystallographic planes for ZIF-8 and ZIF-67, indicating their intact structure and phase composition. The XRD investigation shows that the ZIF-8/ZIF-67 composite maintains its crystallinity despite modifications, as evidenced by its comparable peak characteristics.

Keywords: electrode; nickel foam; metal organic framework (MOF), Zeolitic Imidazolate Framework (ZIF); supercapacitor.

Introduction

The progress of human technology has brought advantages and challenges, including a higher energy requirement. Technological advancements fuel an ever-growing energy demand. The rising energy consumption comes with a cost, as a large amount of energy is wasted due to inefficiencies in its transmission, storage, and use. Ironically, we waste a massive amount of energy while trying to meet our increasing energy demands¹. Energy waste is a complex problem caused by old infrastructure, producing more energy than needed, and lacking efficient ways to store it. Energy is lost at all points in the supply

chain, including generation and end use, with electrical grids losing power as heat due to resistance in the wires². Many industrial processes and consumer products overlook optimal energy efficiency, resulting in unnecessary consumption and waste. Progress has been made in tackling this issue, with supercapacitors emerging as a very promising solution.

Supercapacitors, known for their quick charging, high power density, and long lifespan, have become a popular focus of research. These have widespread applications in portable devices, data storage, electric vehicles, and emergency power sources. Capacitors store electrical energy by collecting charges on two separated, insulated surfaces³. Supercapacitors, also known as ultracapacitors, are high-capacity capacitors with significantly larger capacitance than solid-state capacitors, but they operate at lower voltage limits. This technology combines aspects of both electrolytic capacitors and rechargeable batteries. It offers significantly higher energy density compared to electrolytic capacitors, delivers charge at a much quicker rate

*Corresponding Author: I.L. Ikhioya, ORCID: 0000-0002-5959-4427 Email: imosobomeh.ikhioya@fulokoja.edu.ng



DOI:10.62110/sciencein.mns.2025.v12.1193 URN:NBN:sciencein.mns.2025.v12.1193 © Authors, The ScienceIn https://pubs.thesciencein.org/jmns



than batteries, and boasts a superior lifespan with many more charge-discharge cycles than rechargeable batteries⁴. The main advantage of supercapacitors is their ability to provide high power, surpassing batteries, a key factor in applications requiring rapid energy release. They're also more compact, last longer, and are resistant to temperature changes, which are beneficial in diverse environments. Supercapacitors differ from batteries by storing energy using static electricity, not chemical reactions, resulting in a more reliable performance unaffected by temperature variations⁵. A supercapacitor's core components include electrode material, electrolyte, separator, and collector. Supercapacitor performance is largely determined by the electrode material used.

ZIFs, a subclass of MOFs, are porous crystalline materials created by coordinating metal ions with organic ligands. ZIFs, named for their zeolite-like structures, are formed by combining metal ions (like zinc or cobalt) with imidazolate linkers, creating a porous crystalline structure ⁶. Their tetrahedral coordination of transition metal ions connected by imidazolate linkers, which confer remarkable thermal and chemical stability, characterizes them. Zeolitic Imidazolate Framework-8 (ZIF-8), a metalorganic framework (MOF), has gained widespread recognition in materials science. ZIF-8, possessing a distinctive sodalite (SOD) structure, comprises zinc ions linked with 2-methylimidazole ligands, resulting in a zeolite-like topology. ZIFs share similarities with zeolites due to their metal-imidazole-metal angle mimicking the Si-O-Si angle, resulting in a zeolite-like framework enhanced by MOF characteristics, including high porosity and adjustable pore sizes.

ZIF-8's wide range of applications and the constant research into its capabilities demonstrate its remarkable versatility. 6-8 ZIF-8's potential in fields like environmental sustainability and medical advancements showcases the dynamic nature of MOFs and their role in advancing material sciences. ZIF-67, a zeolitic imidazolate framework, stands out as a captivating material in materials science 9. This is a specific type of metal-organic framework (MOF) that's known for its unique structure, which is very similar to zeolites. ZIF-67's framework uses tetrahedrally-coordinated cobalt ions connected by imidazolate bridges. ZIF-67's robust porosity and remarkable chemical stability, achieved through this configuration, make it ideal for gas storage, separation, and catalytic applications.

As far as we know, the design of ZIF-8/ZIF-67 nanocomposites for supercapacitor applications have been largely overlooked. ZIF-8 nanocomposites decorated with ZIF-67 have been synthesized, characterized, and successfully applied in supercapacitor technology. The ZIF-67/ZIF-8 nanocomposite shows enhanced bandgap and thermal stability compared to pure ZIF-8. The high transmittance observed in optical studies indicates that the composite prioritizes structural integrity over pure electrical conductivity, ¹⁰ resulting in enhanced stability but potentially compromising peak capacitance and charge storage capabilities.

We achieved the synthesis of ZIF-8, ZIF-67, and a ZIF-8/ZIF-67 composite. These materials are finding use in energy storage devices. We comprehensively analyzed these nanocomposites

using multiple electrochemical techniques, such as stability tests, GCD, CV, and EIS. We employed characterization techniques including SEM and XRD. Combining these methods allows us to analyze capacitance, charging/discharging times, power and energy density, cycle life, structure, and chemical makeup. This work cleverly blends ZIF-8/ZIF-67, leveraging their great conductivity, large surface area, and flexibility. This material structure is anticipated to improve charge storage capacity, conductivity, and cycling stability. Synthesis method selection greatly affects the final properties of supercapacitors, such as particle size, shape, purity, and structural soundness. This research aims to address energy storage limitations by enhancing electrode materials through optimized factors, improved electrochemical performance, and enhanced structural stability.

MATERIALS AND METHODS

The reagents for making ZIF-8, ZIF-67, and ZIF-8/ZIF-67 were sourced from Sigma Aldrich. 2-Methylimidazole 98%, Zinc nitrate hexahydrate (Zn(NO₃)₂.6H₂O) 98%, TEA (Triethylamine) 99.5%, and distilled water. The synthesis of ZIF-67 involved the use of the following chemicals: 2-methylimidazole, Cobalt nitrate hexahydrate (Cu(NO₃)₂.6H₂O). The chemical method of synthesis was a direct combination method of synthesis, particularly the mix-and-wait method. The process includes combining the compounds in a precise ratio to create the desired compound. The synthesis process involves direct mixing of a solution of imidazole compound and solutions of zinc or cobalt compounds for ZIF-8 & ZIF-67, respectively, along with the TEA. In this process, the mixture is allowed to sit while the elements combine and can be done at room temperature without the use of any special equipment, making it simple, cheap, and straightforward, producing high-purity products.

2.1 Synthesis of ZIF-8

1.242 g of 2-methylimidazole was dissolved in 50 ml of distilled water in a 100-ml beaker, forming a colorless solution. 1.487 g of (Zn(NO₃)₂.6H₂O) was also dissolved in 50 mL of distilled water in a 100-mL beaker, forming a colorless solution. The resulting solutions are mixed in a 250-mL beaker and stirred for 20 minutes with a magnetic stirrer, forming a white solution. 4 mL of TEA was added in drops to the solution and stirred for another 50 minutes.

2.2 Synthesis of ZIF-67

A colorless solution was formed by dissolving 1.242 g of 2-methylimidazole in 50 mL of distilled water in a 100-mL beaker. Dissolving 0.914 g of (Co(NO₃)₂.6H₂O) in 50 mL of distilled water in a 100-mL beaker resulted in a pink solution when mixed in a 250-mL beaker and stirred for 20 minutes using a magnetic stirrer. After that, 4 mL of TEA was added drop-wise and stirred for another 50 minutes.

2.3 Experimental Procedure-ZIF 8

The process starts with combining 2-methylimidazole with distilled water and then adding solutions of Zinc nitrate hexahydrate. By adding TEA drop by drop to the solution, the formation of nanoparticles was improved as it coordinated with metal ions, influencing the arrangement of organic linkers around the metal ions and enhancing the pore size, crystallinity, and

shape of the ZIF structure. The mixture is stirred with the help of a magnetic stirrer in Figure 1. Afterward, the mixture is transferred to a centrifuge machine for a 10-minute separation process. By using decantation, the mixture is separated, with the colorless solution removed and a white, paste-like residue remaining. The residue is cleaned of contaminants by rinsing it with distilled water and then spun in the centrifuge machine for 10 more minutes. Two additional rounds of washing are carried out. The paste-like remains, separated, were accumulated in a petri dish and then dried in an oven at a temperature of 70 degrees. Stage I of Figure 1 illustrates the dissolution of 2-methylimidazole, zinc salt, and their combinations. A stage II & III centrifuge is used for separation, and an oven for drying of the synthesized material.



Figure 1: Synthesis process of ZIF-8.

2.4 Experimental Procedure-ZIF-67

ZIF-67's experimental procedure is comparable to ZIF-8's, involving similar chemical components and synthesis techniques. Combine a solution of 2-methylimidazole with a solution of cobalt nitrate hexahydrate in a 100-mL beaker. TEA is dripped into the solution for the same purpose as in ZIF-8, resulting in a purple mixture. The combination is stirred with the help of a magnetic stirrer. After stirring thoroughly, the mixture is centrifuged for 10 minutes at 6000 revolutions per minute. The mixture is divided by the centrifuge into a clear solvent and a deep purple residue in Figure 2. The solution is separated, and the leftover substance is cleansed with distilled water before being

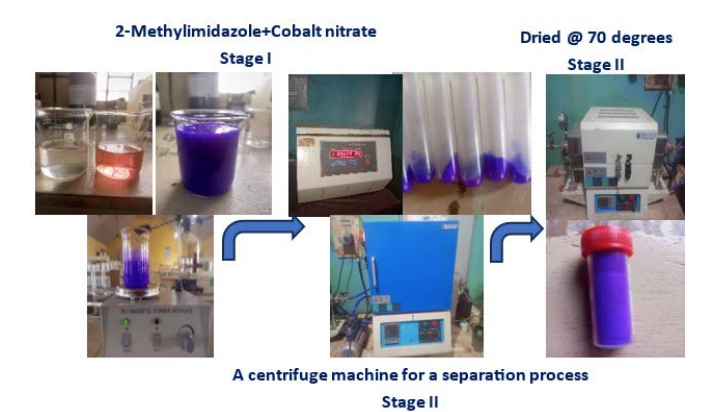


Figure 2: Synthesis process of ZIF-67

spun in the centrifuge apparatus to get rid of any unwanted particles. The washing procedure is repeated twice, and then the resulting mixture is separated by decanting the distilled water. The leftover material is gathered in a petri dish before being dried in an oven at 70 degrees. Stage I of Figure 1 illustrates the dissolution of 2-methylimidazole, cobalt salt, and their combinations. A stage II & III centrifuge is used for separation, and an oven for drying of the synthesized material.

2.5 Experimental Procedure of ZIF-8/ZIF-67 composite

2-Methylimidazole is first mixed with distilled water and combined with a solution of (Zn(NO₃)₂.6H₂O). TEA was added in drops to the resulting solution to improve the nanoparticle formation by coordinating with the metal ions and influencing the assembly of organic linkers around the metal ions, creating better pore size, crystallinity, and shape of the ZIF structure. The experimental procedure of ZIF-67 is similar to that of ZIF-8, as both involve similar chemical materials and synthesis methods. Solutions of 2-Methylimidazole, (Cu(NO₃)₂.6H₂O), combined in a 250-mL beaker. TEA is added in drops to the solution for the same reasons as in ZIF-8, producing a purple mixture. The two solutions were combined to form a solution for the composite of ZIF-8/ZIF-67. The mixture is stirred using a magnetic stirrer. After being thoroughly stirred, the mixture is centrifuged for 10 minutes at 6000 rev/min The centrifuge separates the mixture into a colorless solvent and a dark purple residue. The mixture is decanted, and the residue is washed using distilled water by placing the mixture in the centrifuge machine to remove contaminants. The washing process is also repeated 2 times, and the resulting mixture is separated by decanting the distilled water (See Figures 1 &2). The residue is then collected in a petri dish and placed in an oven to dry at 70 °C.

2.6 Characterization

The electrodes' characteristics were examined through a range of techniques, including optical, structural, morphological, and electrochemical evaluations. The UV-1800 series spectrophotometer was utilized to assess the optical characteristics of the materials. The structural properties were assessed using X-ray diffraction, and the morphological properties were analyzed with SEM. The FTIR spectrometer was utilized for examining the chemical bonds and functional groups present in the materials.

2.7 Electrochemical measurements

The electrochemical analysis was conducted using electrochemical impedance spectroscopy (EIS), galvanostatic charge-discharge (GCD), and cyclic voltammetry (CV) to analyze the charge storage behavior of the prepared electrode. Using the Biologic Potentiostat and EC-Lab Software, the analysis was conducted with a 3-electrode configuration. In the experimental design, a working electrode, reference electrode (Ag-AgCl), and counter electrode were used in a 2M KOH solution. Testing for the EIS involved trying different points, with a frequency range of 1.0 Hz to 105 Hz and an applied potential of 0.7 V.

RESULTS AND DISCUSSIONS

3.1 Electrochemical analysis

Figure 3 (a-c) shows the CV curves for ZIF-8, ZIF-67, and ZIF-8/ZIF-67. The presence of a redox peak in the CV plot indicates the possibility of faradaic reactions. Figure 3 was created from the performance evaluation with scan rates of 1, 5, 15, and 25 mVs⁻¹. The potential ranges of ZIF-8 and ZIF-67 (-0.6 to 0.6 V) and ZIF-8/ZIF-67 (0.0 to 0.5 V) showed substantial peaks in electrode reduction/oxidation, indicating outstanding pseudo-capacitive performance. ZIF-8 and ZIF-67 have computed specific capacitances of (223, 177, 114, and 106) F/g and (255, 187, 142, and 102), respectively. The specific capacitances of ZIF-8/ZIF-67 are (609, 250, 197, 142) F/g. Cyclic voltammetry was used to explore the electrochemical characteristics of electrodes produced at various voltage levels ^{3,4,11-13}. Equation (1) ^{1,9,14-16} was used to determine the specific capacitance.

$$C_S = \frac{\oint I(V)dV}{2AVSm} \tag{1}$$

where C_s , I, s, m, and ΔV are the specific capacitance, the current, scan rate, active, deposited mass, and potential window, respectively. When potential is applied to the material, it exhibits pseudo-capacitive behavior.

Figure 3 (d) shows galvanostatic charge-discharge curves that highlight the electrodes' charging and discharging speeds. Every electrode revealed the same observed forms. Equation (2) 1,9,14–16 was used to determine the specific capacitance.

$$C_s = \frac{I\Delta t}{\Delta vm} \tag{2}$$

Specific capacitance, Cs (F/g), is determined by the discharge current, 1 (A), and the discharge time, Δt (s), while the electrode mass, m (mg), and the potential window during discharge, ΔV (V), also play a role.

Figure 3(d) depicts the galvanostatic charge-discharge plots, which demonstrate the rate of electrode charging and discharging. The galvanostatic charge-discharge method is useful for determining electrode-specific capacitances, energy, and power densities. The ZIF-8, ZIF-67, and ZIF-8/ZIF-67 electrodes have specific capacitances of (79, 194, and 345) F/g at current densities of 1 A/g according to the GCD calculation. Energy densities were obtained by utilizing equation (3) 1,9,14-16.

$$E_D = \frac{1}{2 \times 3.6} C_S \Delta V^2 \tag{3}$$

where C_S (F/g) is the specific capacitance obtained from GCD curves, and ΔV denotes the potential window. Power densities of the electrodes were calculated using the following equation (4):

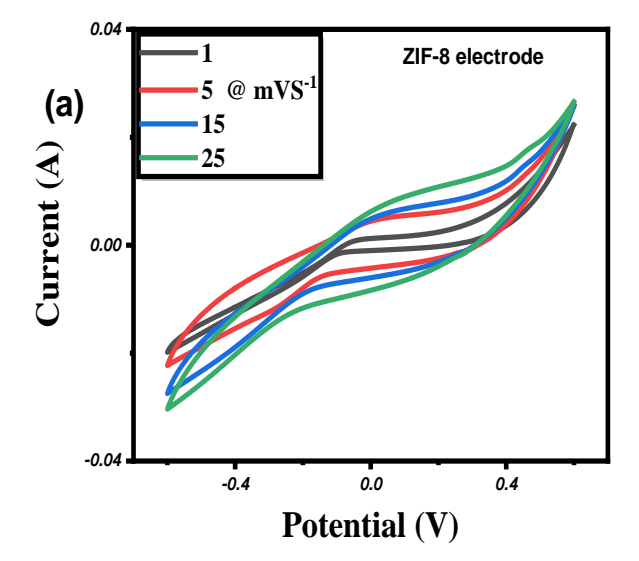
$$P_d = 3.6 \times \frac{E_D}{\Lambda t} \tag{4}$$

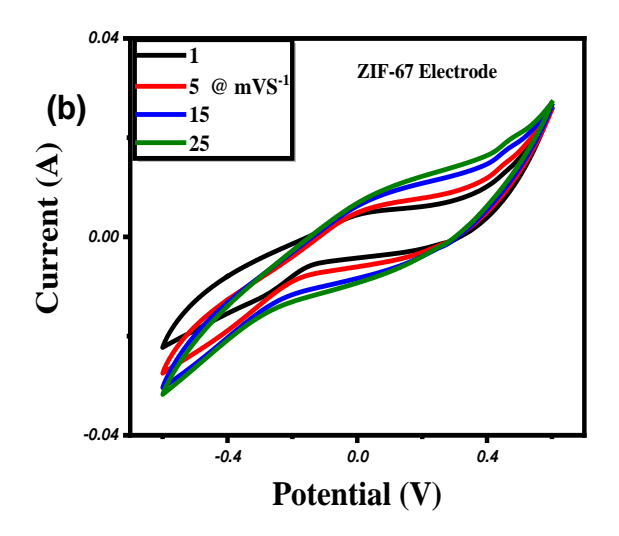
 E_D is the energy density that is calculated from equation (3) $^{1,9,14-16}$, and Δt is the discharge time that will be calculated from GCD curves. The ZIF-8, ZIF-67, and ZIF-8/ZIF-67 electrodes had energy densities of 15.8, 38.8, and 69 Wh/kg, respectively. The power density of ZIF-8, ZIF-67, and ZIF-8/ZIF-67 electrodes was determined to be (469.41, 745.64, and 779) W/kg

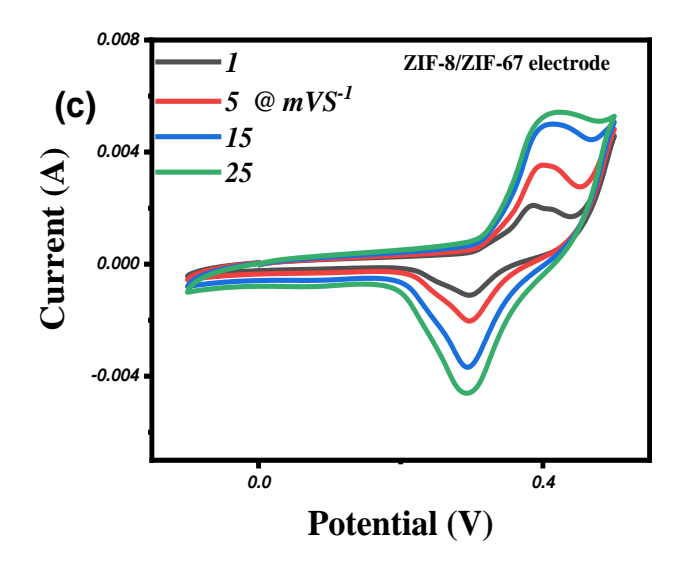
at a current density of 1 A/g. Electrode efficiency was measured using the Coulombic efficiency (η) measure, which measures the efficiency and rate of charge transfer in an electrode. Equation (5) was used to compute the electrodes' efficiency¹⁷.

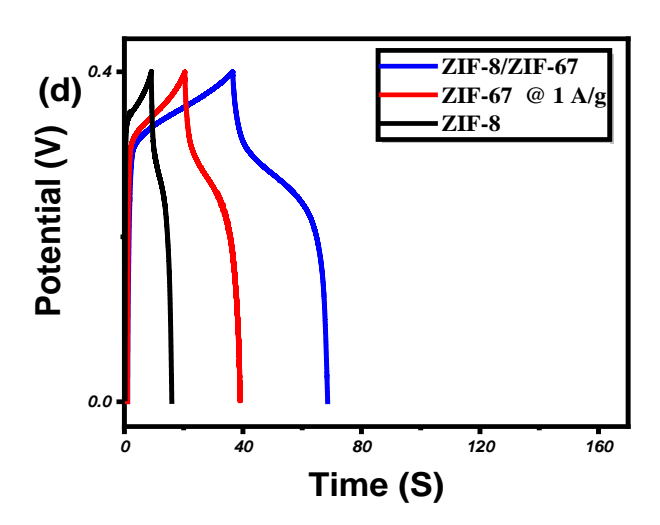
$$\eta = \frac{T_d}{T_c} \qquad x \ 100\% \qquad (5)$$

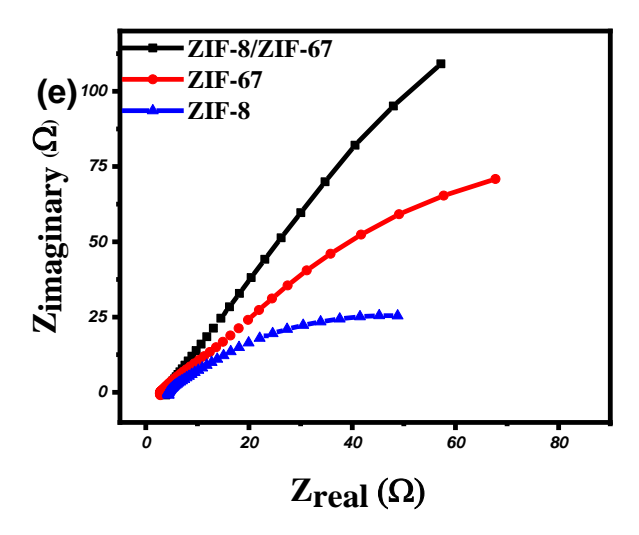
Td and Tc denote the time for charging and discharging, respectively. The retention plot of ZIF-8, ZIF-67, ZIF-8/ZIF-67 electrode in Figure 3 (f) shows efficiency of 65%, 92% and 63%, respectively, indicating their suitability for supercapacitor applications. The impedance of electrochemical systems and the resistance level of the electrode were measured using EIS spectroscopy. Figure 3(e) depicts the EIS results for the built electrodes, which were displayed using Nyquist. A solution resistance (R1) is connected in series to the parallel connection of a constant phase element (CPE or Q), while a charge transfer resistance (R2) is connected in series to a Warburg element.











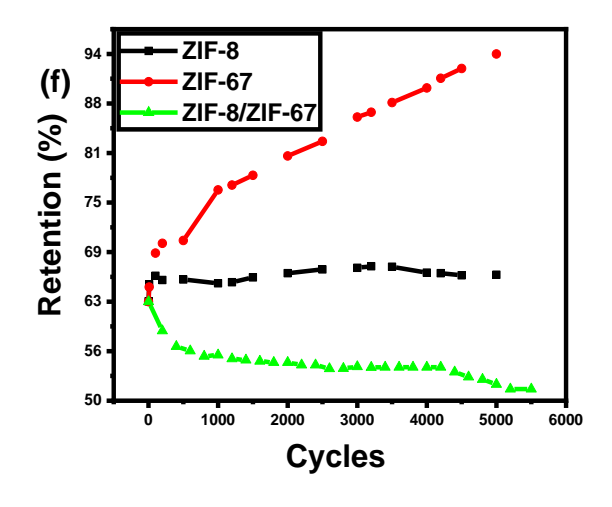


Figure 3:CV of ZIF-8, ZIF-67, and ZIF-8/ZIF-67 composite (a to c), galvanostatic charge discharge plots (d), Nyquist plots (e), and retention plots of ZIF-8, ZIF-67, and ZIF-8/ZIF-67 composite.

3.2 Optical features of ZIF-8/ZIF-67 composite.

The UV-Vis absorbance spectrum of ZIF-8 reveals electronic changes occurring within the material. Absorbance peaks indicate electron activation as they move from lower to higher energy levels. Figure 4 (a) shows a strong peak in absorbance from 950 to 980 nm. This peak represents specific electronic shifts in the material, which are typically associated with charge transfer events or ligand-to-metal charge transfers between zinc ions and imidazolate ligands. The peak's presence in the nearinfrared range indicates that ZIF-8 has vibrational modes or electronic states that are active in this region, which are related to the bending or stretching of chemical bonds within the structure. The absorbance spectra of ZIF-67 show peaks at 950 to 980 nm wavelengths, indicating a link between electronic transitions and ligand-to-metal charge transfer. This zone corresponds to discrete electrical shifts in the substance. ZIF-67 is linked to d-d transitions of zinc ions or charge transfer events involving imidazolate ligands. The peak represents ligand field splitting, which affects the energy levels of the metal ions' dorbitals due to neighboring ligands. The absorbance measured in this region indicates that ZIF-67 is a potential material for photophysical applications, such as photovoltaics photocatalysis, by enhancing performance via near-infrared light absorption. Climbing to the top of this range provides significant information about ZIF-67's structural strength. Modifications to peak intensity or position cause modifications in the structure, affecting its stability and functionality. The presence of different metal centers causes the peaks in the absorbance spectrum to fluctuate in wavelength slightly. The absorbance peaks shift compared to ZIF-8, indicating a probable smaller band gap (~2.7 eV) due to cobalt's d-orbitals ^{1,9,14–16}. The interplay between zincbased ZIF-8 and cobalt-based ZIF-67 gives rise to the distinctive optical features. The absorbance spectrum reveals features of both components. Peaks in the absorbance spectrum coincide with electronic transitions. The ZIF-8/ZIF-67 composite exhibited shifts in peak positions or variations in intensity when

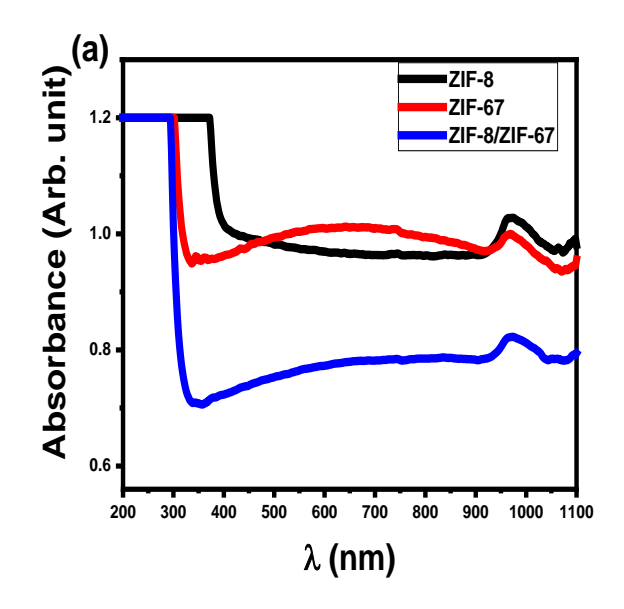
compared to the individual frameworks. This represents the emergence of new electronic states or the effect of one framework on the electronic properties of another. The interactions between ZIF-8 and ZIF-67 produce hybridization effects, which alter the material's electrical characteristics. The absorbance spectrum displays novel absorption characteristics or intensity levels. The spectra are critical for gas adsorption, energy storage, catalysis, and photonic devices because they correspond directly to the electronic characteristics of materials.

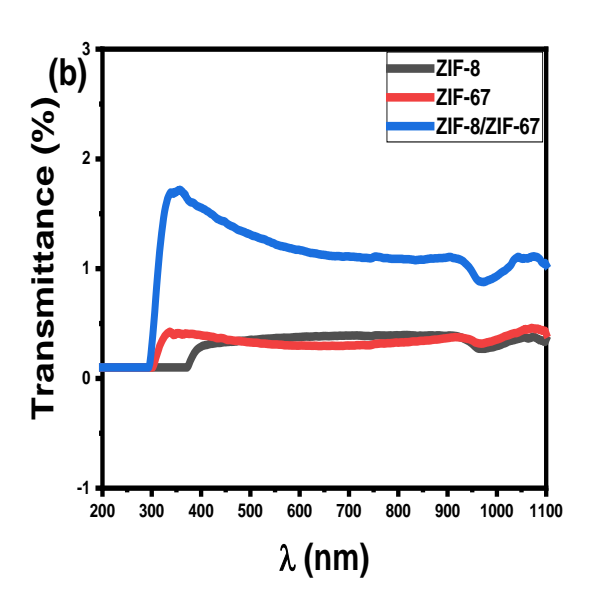
Figure 4 (b) shows a significant drop in transmittance between 200 and 300 nm due to electronic transitions in the imidazolate linkers, resulting in high absorbance. ZIF-8 allows visible light to pass, which makes it ideal for light transmission applications. ZIF-67, like ZIF-8, has outstanding transmittance in the visible spectrum. However, cobalt causes modest changes in transmission characteristics, which may result in absorption patterns at shorter wavelengths due to Co-related transitions. The transmittance spectrum shows poorer transmittance than ZIF-8, particularly in the UV band. The ZIF-8/ZIF-67 combination changes the transmittance spectrum. Transmittance decreased compared to pure ZIF-8, particularly in the UV band, as the materials absorbed light via f-f transitions. The visible region has good transmittance; however, the overall profile differs slightly from ZIF-8/ZIF-67 due to the unique framework structures of ZIF-67. ZIF and ZIF-67 are excellent candidates for optical applications due to their high transparency in the visible region. The presence of zinc and cobalt ions in ZIF-8 and ZIF-67 composites enhances UV transmission. ZIF-67's transmittance is lowered due to added absorption properties that differ depending on the metal center. The transmittance spectra are important for sensors, catalysis, and photonic devices because they reveal how materials react to light.

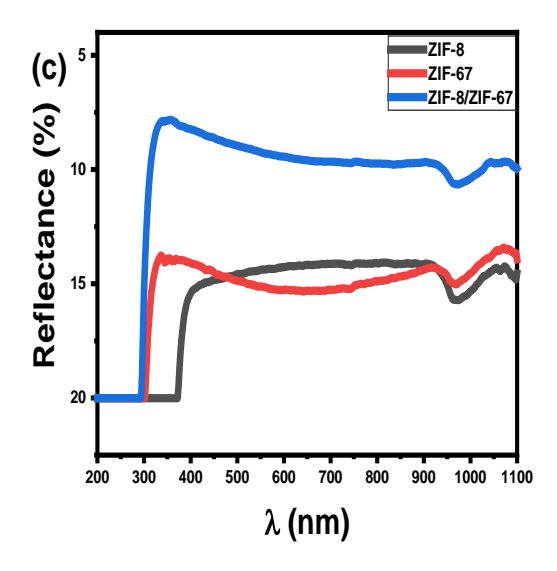
ZIF-67 has a somewhat higher reflectance than ZIF-8, particularly in the UV region, due to the cobalt component, which provides additional electronic transitions in Figure 4 (c). The ^{1,12,26,18–25}of reflectance co-related transitions differences in spectral feature peaks when compared to ZIF-8. ZIF-67, like ZIF-8, has low reflectance in the visible range 1,9,14-¹⁶. The variable metal compositions (Zn for ZIF-8 and Co for ZIF-67) influence their optical properties and possible uses in a variety of disciplines. Reflectance analysis in the ZIF-67/ZIF-8 composite reveals changes in band edges, implying enhanced photovoltaic efficiency in visible light, which is an important element in improving materials for energy conversion. ZIF-8 (Zinc-based) and ZIF-67 (Cobalt-based) have different electrical structures, which influence their light absorption and reflection. The composites' reflectance demonstrates how different metal ions interact and influence the overall optical behavior. The reflectance spectrum can be used to evaluate the composite's band gap energy. Lower reflectance in specific locations indicates increased absorption, demonstrating effective light consumption in solar applications.

The bandgap energies of ZIF-8 (2.50 eV) and ZIF-67 (2.77 eV) indicate their potential as semiconductors in electronic applications, with ZIF-67 having a higher energy and thus greater electronic characteristics in Figure 4 (d). The composite ZIF-

8/ZIF-67 has a reduced bandgap (2.35 eV), indicating increased charge carrier mobility due to the mixing of frameworks.ZIF-8's (2.50 eV) value indicates that it absorbs light from the ultraviolet to the visible spectrum, making it potentially helpful in applications ^{27–37}. Its bandgap indicates modest semiconductor characteristics, which allows for some charge carrier mobility. The greater bandgap energy of ZIF-67 (2.77 eV) indicates that it has stronger electronic characteristics than ZIF-8. This translates to greater stability against photo-induced deterioration and, potentially, increased efficiency in applications demanding higher energy transitions ^{18–20,22,23}. The ZIF-8/ZIF-67 Composite (2.35 eV) bandgap indicates that the combination of ZIF-8 and ZIF-67 results in better charge carrier mobility and lower recombination rates. This improves the material's energy storage efficiency and qualifies it for applications where adjustable electronic characteristics are advantageous.







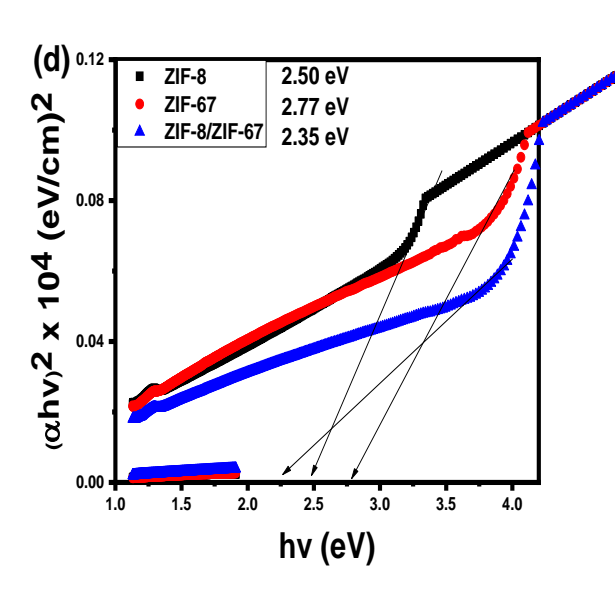


Figure 4: absorbance (a), transmittance (b), reflectance (c), and energy bandgap (d) of ZIF-8, ZIF-67, and ZIF-8/ZIF-67 composite.

3.3 FTIR study of ZIF-8/ZIF-67 composite

Figure 5 shows ZIF-8's FTIR spectrum, which shows a significant C=N stretching vibration at 1583 cm⁻¹ and ring stretching peaks between 1444-1383 cm⁻¹. These properties indicate imidazolate linkers unique to ZIF-8. The FTIR spectrum of ZIF-67 reveals comparable characteristic peaks with minor changes due to its unique metal and ligand composition. Examination reveals information on the differences in structure and bonding environments. The composites exhibit changes in peak locations and intensity, indicating interactions between ZIF-8 and ZIF-67 that enhance their effectiveness in applications. The C=N stretching vibration at 1583 cm⁻¹ shows in idazolate linkers. The peaks at 1444-1383 cm⁻¹ indicate C -C stretching vibrations in the imidazolate ring. Metal coordination produces lower frequency bands (600-800 cm⁻¹), showing the

framework's structural strength. ZIF-67 has a C=N stretching peak similar to ZIF-8, but with slightly altered wave numbers assigned to Cobalt. The spectrum differs in intensity and location from ZIF-8, demonstrating ZIF-67's unique bonding characteristics. The peaks from the imidazolate linkers will also appear, albeit in a somewhat different position. The detected shifts in the composite spectrum indicate interactions between ZIF-8 and ZIF-67 ³⁸. Changes in the strength of individual peaks indicate the formation of new bonds or interactions in the composite structure. The appearance of additional peaks implies the formation of hybrid structures or altered environments around the functional groups.

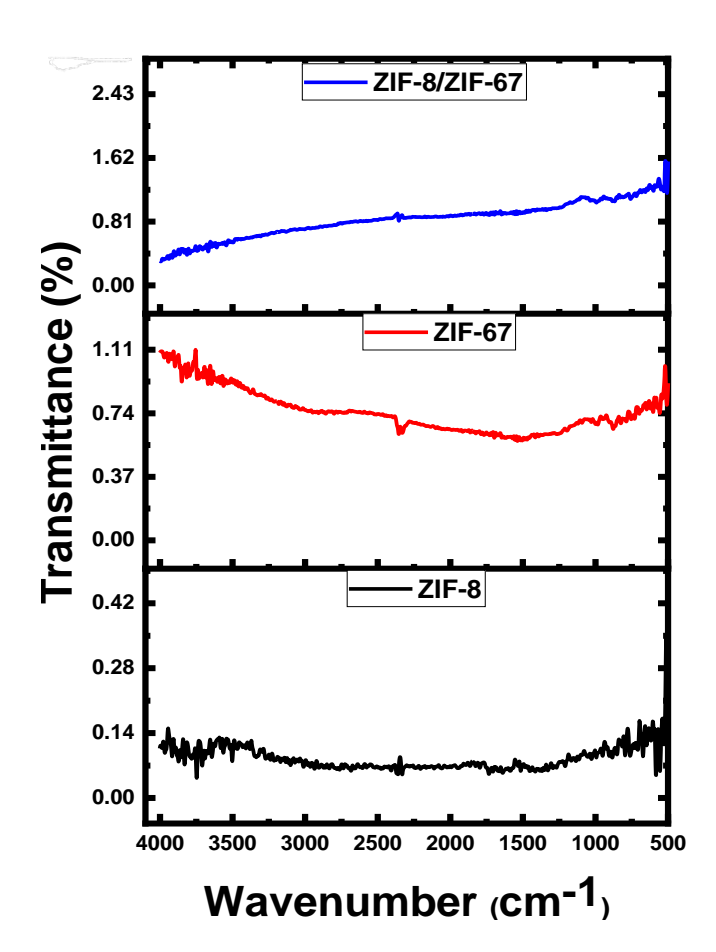


Figure 5: FTIR spectrum of ZIF-8, ZIF-67, and ZIF-8/ZIF-67 composite.

3.4 X-ray diffraction study of ZIF-8/ZIF-67 composite

Figure 6 shows that the XRD diffraction peaks at 22.09° (110), 26.62° (200), 38.49° (211), and 47.27° (220) correspond to unique crystallographic planes for ZIF-8 and ZIF-67, indicating their intact structure and phase composition. The XRD investigation demonstrates that the ZIF-8/ZIF-67 composite has comparable peak characteristics, indicating that crystallinity is preserved despite modifications. This peak represents the (110) crystallographic plane, which is unique to the framework structures of ZIF-8 and ZIF-67. It indicates a precise organization and consistency in the material's composition. The peak at 200

on the graph indicates a higher level of structural complexity. The zeolitic framework's packing efficiency and symmetry repeatedly demonstrate its usefulness in energy storage applications. The existence of the (211) plane implies complex structural properties. This peak represents the interlayer spacing and connectivity in the framework, which influences the material's adsorption characteristics. The existence of the (220) peak indicates a well-defined crystal structure with higher-order reflections. The prominent peaks show that ZIF-8 and ZIF-67 have good crystallinity. Peak sharpness and intensity represent the quality of the crystalline structure. The presence and nature of these peaks in the ZIF-8/ZIF-67 composite indicate that the individual ZIF components' structural integrity is maintained. This implies that the composite creation does not alter the crystalline structure. The peaks associated with these planes indicate that ZIF-8 and ZIF-67, as well as their combination, are stable under the study conditions. Catalysis and energy storage rely heavily on stability. The intensity and placement of peaks in ZIF-8, ZIF-67, and their composite can be used to determine how these frameworks interact. Shifts in peak intensity indicate structural changes or the formation of new phases in the composite.

The 2 theta diffraction angles of ZIF-8 and ZIF-67 provide vital information about their structural features and stability. The angles 22.09°, 26.62°, 38.49°, and 47.27° are distinct peaks indicating crystallites in ZIF-8 and ZIF-67 composites, which are critical for catalysis and energy storage applications. According to studies, the conditions under which ZIF-8 and ZIF-67 are synthesized determine their average particle size, with smaller crystallite sizes resulting in higher surface areas and better gas interaction. The material's performance is affected by noticeable differences in diffraction patterns at specific angles. ZIF-8/ZIF-67 mixed-metal composites produce precise crystallite sizes that increase surface properties, hence improving material features for selective gas adsorption in storage applications. The diffraction data show that these composites have high structural integrity. A particular plane in ZIF-8 is related to crystallite sizes of 0.2362 nm. Smaller values for crystallite size often indicate denser atom packing, which is linked to smaller crystallite sizes. This suggests that ZIF-8 has a basic crystal structure, which contributes to its large surface area and porosity. ZIF-67 is related to crystallites of 0.2381 nm. The small increase in crystallite sizes as compared to ZIF-8 suggests differences in metal centers and ligand combinations that influence crystallite size. The simpler framework structure of ZIF-67 results in bigger crystallite sizes. Crystallite sizes of 0.2458 nm and 0.2537 nm suggest that the composite material shares features with both ZIF-8 and ZIF-67. Differences in crystallite sizes indicate that the interaction of the two frameworks may result in structural modifications that improve attributes like as stability and energy storage capacity. Smaller crystallite sizes enhance surface area, which improves reactivity and adsorption. Crystallite size values provide insight into how these materials are optimized for application in catalysis, energy storage, and separation processes. The various crystallite sizes in the composite indicate that the integration of ZIF-8 and ZIF-67 was successful, resulting in increased material strength and performance.

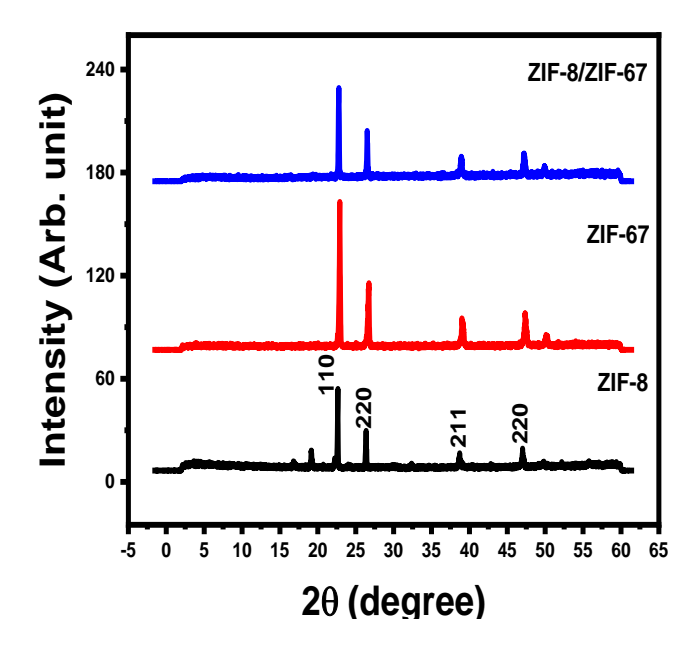


Figure 6: XRD pattern of ZIF-8, ZIF-67, and ZIF-8/ZIF-67 composite.

3.5 Surface morphological study of ZIF-8/ZIF-67 composite Figure 7 depicts the distinct surface features of ZIF-8 and ZIF-67. ZIF-8 has a definite structure with consistent particles, but ZIF-67 has a variable crystalline form, which affects its efficiency. The surface morphology of ZIF-8 and ZIF-67 nanoparticles stays unchanged, indicating their resilience. ZIF-8 has a definite and constant particle form, which usually resembles rhombic dodecahedra. This homogeneity accounts for its large surface area and porosity. Its smooth and level surface enhances its ability to absorb, making it ideal for energy storage. ZIF-67, a cobalt-based variant of ZIF-8, has a unique structure with irregular forms and larger particle diameters. The crystal structure changes due to the introduction of cobalt ions. The irregular shape produces unique adsorption properties when compared to ZIF-8, which may affect its stability and interactions with guest molecules. The composite combines structures from ZIF-8 and ZIF-67. The surface combines the smooth, consistent properties of ZIF-8 with the rougher characteristics of ZIF-67. The combination of various morphologies enhances the material's characteristics, such as increased surface area and extensible porosity. By combining the capabilities of both frameworks, the composite may improve performance in energy storage applications. The unique structures of ZIF-8 and ZIF-67 impact their effectiveness; nevertheless, when joined in a composite form, they exhibit increased properties, making them appropriate for a wide range of sophisticated applications. Figure 8 depicts the elemental makeup of ZIF-8, ZIF-67, and the composite (ZIF-8/ZIF-67). The basic components of ZIF-8 are zinc (Zn) ions and imidazolate (C₃H₃N₂) ligands. Its structure is similar to that of zeolite, with Zn atoms organized tetrahedrally,

producing a highly porous substance. ZIF-67 is similar to ZIF-8, with the exception that zinc is replaced with cobalt (Co) ions while the imidazolate ligands remain the same. The structure is tetrahedral as well; however, Co alters the electrical properties and improves catalytic activity. Because of its unique redox characteristics, ZIF-67 is stable and has been investigated for potential applications in catalysis and as an electrode material. The composite structure combines Zn and Co ions, integrating components from both ZIF-8 and ZIF-67. The composite exhibits a blended structure, resulting in specific traits not found in the individual phases. Combining them improves a variety of features, including enhanced porosity and combined effects, which improve performance in energy storage applications. The composite benefits from the combination of Zn and Co, which increases its functionality.

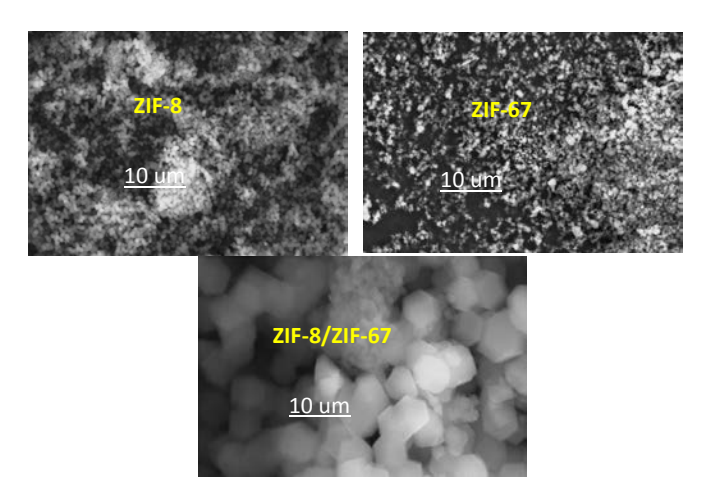
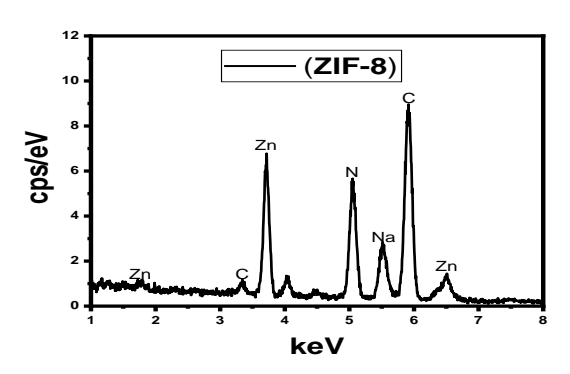
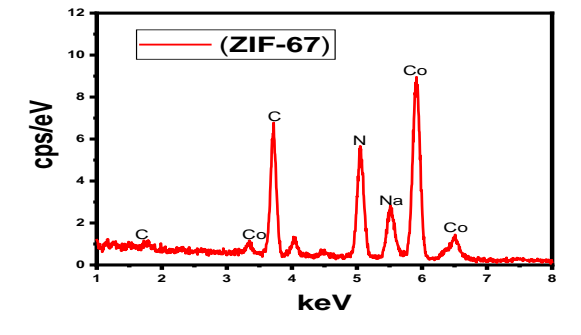


Figure 7: surface micrograph of ZIF-8, ZIF-67, and ZIF-8/ZIF-67 composite.





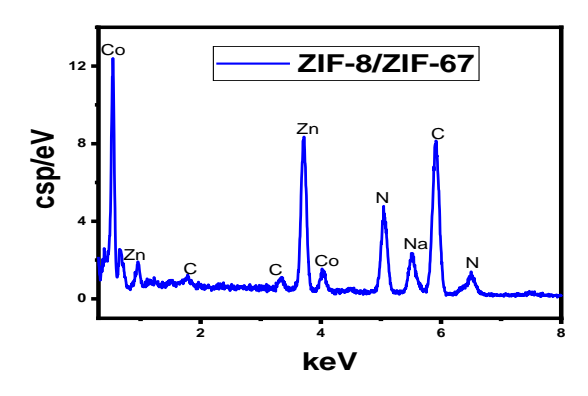


Figure 8: EDX plots of ZIF-8, ZIF-67, and ZIF-8/ZIF-67 composite.

CONCLUSIONS

We have successfully used a direct combination method of synthesis ZIF-8, ZIF-67, and a ZIF-8/ZIF-67 composite. The absorbance spectra of ZIF-67 show peaks at 950 to 980 nm wavelengths, indicating a link between electronic transitions and ligand-to-metal charge transfer. This zone corresponds to discrete electrical shifts in the substance. ZIF-67 is linked to d-d transitions of zinc ions or charge transfer events involving imidazolate ligands. The peak's presence in the near-infrared range indicates that ZIF-8 has vibrational modes or electronic states that are active in this region, which are related to the bending or stretching of chemical bonds within the structure. ZIF-8's FTIR spectrum, which shows a significant C=N stretching vibration at 1583 cm⁻¹ and ring stretching peaks between 1444-1383 cm⁻¹. These properties indicate im idazo late linkers unique to ZIF-8. The FTIR spectrum of ZIF-67 reveals comparable characteristic peaks with minor changes due to its unique metal and ligand composition. Examination reveals information on the differences in structure and bonding environments.

AUTHOR CONTRIBUTION STATEMENT

Ekene Uduike, Oparaku, Emeka, Imosobomeh L. Ikhioya, Chidiebere O. Obasi: methodology, conceptualization, data curation, data collection, Chidiebere O. Obasi, Imosobomeh L. Ikhioya: samples characterization, first-draft writing, software, reviewing, and editing. Oparaku, Emeka, Imosobomeh L. Ikhioya, supervisor, investigation and visualization. All authors approved the submission of the manuscript.

DISCLOSING CONFLICTING INTERESTS.

The authors of this paper declare that there are no personal or financial conflicts that may have affected the study.

Availability of data

Access to the data is available upon request.

REFERENCE

- I.L. Ikhioya, N.Z. Ali, S. Tahir, et al. Electrochemical engineering of ZIF-7 electrode using ion beam technology for better supercapacitor performance. J. Energy Storage 2024, 90, 111833.
- X. Li, X. Yang, H. Xue, H. Pang, Q. Xu. Metal-organic frameworks as a platform for clean energy applications. *EnergyChem* 2020, 2 (2), 100027.
- R.M. Obodo, H.E. Nsude, C.U. Eze, et al. Investigating the Dual Synergistic Amalgamation of CeO2@WO3/GO Electrodes for Supercapacitor Application. *Energy Storage* 2024, 6 (5), 1–12.
- E.U. Onoh, P. Khwesa, I.L. Ikhioya, et al. Experimental and theoretical investigation of high-performance green-synthesized NaTiO2/AC nanocomposite as high-capacity electrodes for next-generation sodiumion capacitors. *J. Mater. Sci.* 2024, 59 (40), 19210–19227.
- I. Rabani, J.W. Lee, T. Lim, et al. Construction of a uniform zeolitic imidazole framework (ZIF-8) nanocrystal through a wet chemical route towards supercapacitor application. RSC Adv. 2024, 14 (1), 118–130.
- F.N. Al-Rowaili, U. Zahid, S. Onaizi, et al. A review for Metal-Organic Frameworks (MOFs) utilization in capture and conversion of carbon dioxide into valuable products. *J. CO2 Util.* 2021, 53, 101715.
- A.M. Aboraia, A.A.A. Darwish, V. Polyakov, et al. Structural characterization and optical properties of zeolitic imidazolate frameworks (ZIF-8) for solid-state electronics applications. *Opt. Mater.* (Amst). 2020, 100, 109648.
- S. Ahmad, M. Tariq, Z.U. Rehman, et al. A tremella-like in situ synthesis of ZIF-67Co(OH)F@Co3O4 on carbon cloth as an electrode material for supercapacitors. RSC Adv. 2024, 14 (38), 27831–27842.
- R.M. Abdelhameed, M. Abu-Elghait, M. El-Shahat. Hybrid three MOFs composites (ZIF-67@ZIF-8@MIL-125-NH2): Enhancement the biological and visible-light photocatalytic activity. *J. Environ. Chem. Eng.* 2020, 8 (5), 104107.
- A. Awadallah-F, F. Hillman, S.A. Al-Muhtaseb, H.-K. Jeong. On the nanogate-opening pressures of copper-doped zeolitic imidazolate framework ZIF-8 for the adsorption of propane, propylene, isobutane, and n-butane. *J. Mater. Sci.* 2019, 54 (7), 5513–5527.
- W.U. Hassan, F. Kaleem, M.R. Mahmood, et al. Enhanced solid-state reaction synthesis of CdO, SnO, and CdOO·2/SnOO.2 hetero-junction electrode for high-performance energy storage. *Chem. Inorg. Mater.* 2024, 4 (November), 100079.
- K. Shahzad, M. Rahim, H.Z. Shafi, A. Shah, I.L. Ikhioya. Impact of reduced graphene oxide on La0.5Ca0.5MnO3 nanocomposite electrode for high-performance energy storage application. *J. Mater. Sci.* 2024, 59 (35), 16644–16659.
- U.I. Courage, N. Alghamdi, I.L. Ikhioya, et al. Investigating the Linum usitatisimum mucilage synergistic amalgamation of metal oxide electrodes for super-capacitive applications. *J. Indian Chem. Soc.* 2024, 101 (12), 101477.
- S. Ibrar, E.O. Ojegu, O.B. Odia, et al. Assessing High-Performance Energy Storage of the Synthesized ZIF-8 and ZIF-67. J. Appl. Organomet. Chem. 2023, 3 (4), 294–307.
- M. Ghafoor, Z.U. Khan, M.H. Nawaz, et al. In-situ synthesized ZIF-67 graphene oxide (ZIF-67/GO) nanocomposite for efficient individual and simultaneous detection of heavy metal ions. *Environ. Monit. Assess.* 2023, 195 (3), 423.
- S. Feng, M. Bu, J. Pang, et al. Hydrothermal stable ZIF-67 nanosheets via morphology regulation strategy to construct mixed-matrix membrane for gas separation. *J. Memb. Sci.* 2020, 593, 117404.
- X. Deng, L. Zhang, J. Guo, Q. Chen, J. Ma. ZnO enhanced NiO-based gas sensors towards ethanol. *Mater. Res. Bull.* 2017, 90, 170–174.
- I.. Agbrara, A.I, Emuvokeraye, O.S, Osiele, M.O, and Ikhioya. Influence of deposition temperature on the bandgap energy and optical characteristics of electrochemically prepared SrSe/ZrSe heterostructure Agbrara, A.I. Niger. J. Sci. Environ. 2025, 23 (1), 134–144.
- N. Alghamdi, I.L. Ikhioya. Improved efficiency of silver incorporation in the lattice of zirconium oxide via hydrothermal process for photovoltaic application. J. Indian Chem. Soc. 2025, 102 (6), 101719.

- I.L. Ikhioya, A.C. Nkele, K. Shahzad, E.O. Ejeh, F.U. Ochai-Ejeh. The effects of nitrogen ions' implantation on La0.5Ca0.5MnO3 nanocomposite electrode for high-performance supercapacitor applications. J. Mater. Sci. Mater. Electron. 2025, 36 (13), 800.
- Q. Yang, Y. Xu. Zeolitic imidazolate framework-67 derivative/TiO2 composite coating as an integrated anode for lithium-ion batteries. *Bull. Mater. Sci.* 2023, 46 (2), 102.
- E.O. Ojegu, B.U. Osolobri, E.I. Onyesom, et al. Yttrium incorporation into the tungsten telluride (Y:WTe2) matrix achieved using three electrode systems. *Mater. Nanosci.* 2025, 12 (1), 1185.
- K. Shahzad, M. Rahim, H.Z. Shafi, A. Shah, I.L. Ikhioya. rGO-Pr0.5Ca0.5MnO3 Nanocomposites: A Path to High-Energy Density Supercapacitors. Arab. J. Sci. Eng. 2025.
- E.O. Okechukwu, I.L. Ikhioya, A.J. Ekpunobi. Effect of precursor pH on the electrochemically synthesised barium titanium sulphide (BaTiS) material for photovoltaic application. *Mater. Res. Innov.* 2024, 00 (00), 1–10
- I.L. Ikhioya, N. Alghamdi, N.M. Ugwu, et al. Fabrication of gadolinium oxide into the matrix of ZIF-67 via direct combination method for energy storage application. *Hybrid Adv.* 2025, 8 (December 2024), 100358.
- F.I. Ijeh, R. O, Ikhioya, L. I, Ezema. Synthesis and characterization of copper doped TiO2 via electrodeposition method for photovoltaic applications. FUPRE J. Sci. Ind. Res. 2024, 8 (4), 339–351.
- I.L. Ikhioya, A.C. Nkele, D.N. Okoli, A.J. Ekpunobi, I. Ahmed. Influence of varying molar concentration on the properties of electrochemically-deposited zirconium-doped ZnSe thin films. *J. Indian Chem. Soc.* 2022, 99 (9), 100641.
- I.L. Ikhioya, A.C. Nkele, D.N. Okoli. Effects of temperature and ph variations on electrochemically-deposited zirconium-doped zinc selenide thin films. Optik (Stuttg). 2022, 260 (September 2021), 169055.
- I. mosobomeh L. Ikhioya, N.I. Akpu, E.U. Onoh, et al. Enhanced physical properties of nickel telluride metal chalcogenide material with molybdenum dopant. *Mater. Res. Innov.* 2024, 28 (1), 40–48.
- I.L. Ikhioya, F.U. Ochai-Ejeh, C.I. Uruwah. Impact of modulated temperature on photovoltaic properties of automated spray fabricated zirconium doped cobalt selenide films. *Mater. Res. Innov.* 2023, 27 (6), 382–391.
- I.L. Ikhioya, E.O. Onah, M. Maaza, F. Ezema. Influence of precursor pH on the optical and electrical properties of electrochemically deposited cobalt-doped ZnSe thin films for photovoltaic application. *Curr. Res. Green Sustain. Chem.* 2022, 5 (December 2021), 100286.
- 32. I.L. Ikhioya, E.U. Onoh, D.N. Okoli, A.J. Ekpunobi. Impact of bismuth as dopant on ZnSe material syntheses for photovoltaic application. *Mater. Res. Innov.* **2023**, 27 (6), 411–419.
- I.L. Ikhioya, C.U. Udeze, F.U. Ochai-Ejeh, et al. Optimization of erbium percentage molarity on cobalt selenide semiconductor material via spray pyrolysis deposition technique for photovoltaic application. *J. Indian Chem. Soc.* 2022, 99 (12), 100793.
- 34. I.L. Ikhioya, C.O. Ugwuoke, R.M. Obodo, et al. Influence of precursor pH on Bi doped ZnSe material via electrochemical deposition technique. *Appl. Surf. Sci. Adv.* **2022**, 9 (November 2021), 100232.
- I.L. Ikhioya, C.O. Ugwuoke, D.N. Okoli, et al. Effect of cobalt on the photovoltaic properties of zinc selenide thin film deposited on fluorinedoped tin oxide (FTO) via electrochemical deposition technique. *Curr. Res. Green Sustain. Chem.* 2022, 5 (May), 100328.
- I.L. Ikhioya, G.M. Whyte, A.C. Nkele. Temperature-modulated nanostructures of ytterbium-doped Cobalt Selenide (Yb-CoSe) for photovoltaic applications. *J. Indian Chem. Soc.* 2023, 100 (1), 100848.
- I.L. Ikhioya, C.O. Ugwuoke, F.U. Ochai-Ejeh. Optimisation of temperature regulator on spray pyrolysis cobalt selenide doped erbium (CoSe: Er) semiconductor material for photovoltaic application. *Mater. Res. Innov.* 2024, 28 (1), 32–39.
- E.O. Ojegu, R.A. Daniel-Umeri, E.C. Nwaokorongwu, N. Alghamdi, I.L. Ikhioya. Optimization of silver ion concentration into the lattice of zinc oxide nanoparticles synthesized via a hydrothermal approach. *Niger. J. Technol. Dev.* 2025, 21 (4), 145–158.